# Carbon dimers on the diamond (100) surface: Growth and nucleation

Michael Sternberg,* Peter Zapol, and Larry A. Curtiss
*Materials Science and Chemistry Divisions, Argonne National Laboratory, Argonne, Illinois 60439, USA*
(Received 17 April 2003; published 25 November 2003)

We use a density-functional based tight-binding method to study diamond growth by $C_2$ on a nonhydrogenated diamond (100)-(2×1) surface. The study is motivated by advances in the growth of ultrananocrystalline diamond (UNCD) films under hydrogen-poor conditions. We identify and classify stable adsorbate configurations formed above dimer rows and troughs on the reconstructed surface. We also investigate adsorption and migration barriers using the nudged elastic band method. We find viable adsorption pathways leading to chain growth and step advancement. Initial depositions proceed without barriers into topologically imperfect configurations. The most stable configuration is a growth position that bridges two adjacent surface dimers along a dimer row. It is reached over a barrier of 1.2 eV and has an adsorption energy of −6.9 eV. Many other configurations exist that have adsorption energies differing by up to 2.7 eV. By comparison, analogous structures for silicon are fewer in number and closer in energy because Si lacks $\pi$ bonding, which is important for $C_2$ on diamond. Migration barriers for ad-dimers are in the range of 2–3 eV due to relatively large differences in the energies of intermediate local minima. Comparing our results with previous studies on the (110) surface, we note that barriers leading to growth are higher and pathways are more complex on the (100) surface. The barriers suggest that reactions leading to both growth and re-nucleation are possible, which helps to understand the small observed grain sizes in UNCD.

DOI: 10.1103/PhysRevB.68.205330 PACS number(s): 68.43.Fg, 61.43.Bn, 81.15.Aa

## I. INTRODUCTION

Reaction mechanisms of diamond growth from hydrogen-poor plasmas should be much different from those in conventional growth regimes. Studies of mechanisms for conventional diamond growth have shown that hydrogen abstraction is an extremely important step and that methyl radicals and acetylene are the dominant growth species.[1–4] These findings help to optimize adjustable parameters for the growth process.

It is expected that under hydrogen-poor conditions at least part of the growing surface will be free of hydrogen. Therefore, it is interesting to investigate whether diamond growth is still possible on nonhydrogenated surfaces. Also, the composition of carbon species in the plasma is rather different. Experimental studies of growth from Ar-$CH_4$ plasmas[5] resulted in unique ultrananocrystalline diamond (UNCD) films. Optical emission studies of the plasma have shown intensive green Swan-band radiation indicating the presence of $C_2$ dimers.[6]

Gruen *et al.*[5,7] also pointed out the link between the small grain size of UNCD and a high renucleation rate. Further, it was recognized that up to 10% of the total amount of carbon in the films is located at 2 to 4 atom-wide grain boundaries. It was proposed that (100)-like surfaces are the most typical surfaces in UNCD.[8,9] Therefore, the processes of growth and nucleation on these surfaces are of primary interest for understanding of the structure and morphology of the resulting films.

The novel mechanisms of diamond growth from $C_2$ species has attracted attention from theorists. The first steps to a detailed understanding of the growth mechanism were taken considering $C_2$ reactions with hydrogen free and monohydrided diamond surfaces. In studies by Horner *et al.*[10,11] it was shown that $C_2$ insertion into C-H bonds on the hydrogenated (110) surface has small activation barriers of less than 0.2 eV and is highly exothermic. Subsequent steps involving linkage of $C_2$ units also have low barriers and lead to growth. In our previous work[12] we considered the hydrogen-free (110) surface and also found stable $C_2$ adsorbate configurations which lead to diffusion-assisted chain growth. It was also found that intermediate graphitization occurs in the form of fullerenelike and nanotubelike fragments on the surface. Nonetheless, such fragments are rebonded to the surface in subsequent growth stages, leading to stable growth on this surface even in the absence of hydrogen.

The growth processes on the unhydrided (100) surface due to $C_2$ has been modeled in its initial stage on cluster models,[7] but a comprehensive study has not yet been performed. The objective of the present paper is to consider $C_2$ reactions with nonhydrogenated (100) surfaces and to find out whether these reactions could result in diamond growth. We calculate optimized structures, adsorption energetics, and reaction pathways to obtain baseline information on growth mechanisms of UNCD.

For a number of adsorbate structures on diamond, analogs also occur on the silicon (100) face. As an aid to understanding the characteristics and bonding situation on diamond we present a comparison against these well-studied cases.

Our computational method is briefly outlined in Sec. II. The main results are given in Sec. III, where we first (Sec. III A) review the properties of the diamond (100) surface as calculated using the density-functional based tight-binding method, including a comparison with more elaborate *ab initio* results. The initial adsorption steps for $C_2$ on diamond (100) are studied in Sec. III B, followed by an evaluation of adsorption barriers in Sec. III C. We discuss the implications of these results in Sec. III D and present a summary in Sec. IV.

 

## II. COMPUTATIONAL METHOD

The density-functional-based tight binding (DFTB) method[13,14] was used for obtaining energies and forces. The method has been successfully applied to a variety of systems, with particular success for carbon.[14]

The method is based on an approximate solution of the Kohn-Sham-like equations using an optimized nonorthogonal atomic basis set. The repulsive atomic pair potentials of the tight-binding formulation are determined beforehand from first-principle calculations. The variation of a density functional expression approximated to second order yields the secular equations which are solved self-consistently for the Mulliken charges. Interatomic forces for total energy minimizations and molecular dynamics are calculated semianalytically as the gradients of the total energy at the atomic positions. Local minima of the total energy have been obtained by a conjugate gradient minimization procedure with a convergence criterion for the maximum force per atom generally not exceeding 5 meV/Å.

We modeled reference structures of the reconstructed (100)-(2×1) diamond surface using two-dimensional (2D) periodic boundary conditions with a supercell containing 16 atoms per layer and 16 monolayers, keeping the bottom layer saturated with two pseudohydrogen atoms per carbon. The pseudohydrogen atoms have their mutual interaction switched off to avoid problems of steric repulsion otherwise arising on a bulklike dihydrogenated termination. The saturation ensures the unreconstructed (1×1) geometry and keeps layer relaxations to a minimum. The interlayer distance between the second and third monolayer from the bottom already deviates by less than 1% from the bulk value.

For the adsorption studies, we use surface models with six monolayers of carbon and a pseudohydrogen saturation layer. Key structures were also calculated with eight carbon monolayers, which resulted in essentially the same energies and geometries for the resulting structures, with changes in adsorption energies of the order of 30 meV.

To calculate adsorption and migration barriers for a $C_2$ molecule on the surface, we have used the nudged elastic band (NEB) method.[15,16] The NEB method aims to find the minimum energy path in coordinate space connecting two fixed states, which usually represent local energy minima. The path is represented by a finite number of system configurations, called *images*, which are connected to their nearest neighbors by an auxiliary spring force. The spring force on each image augments the physical force on each atom given by the negative gradient of its potential energy. In order to avoid certain artefacts a projection method is applied whereby the components of the physical force parallel to the NEB path and spring forces normal to the NEB path are removed. In effect, the total force for all images is then minimized using a simple dynamic algorithm.[16] The method was demonstrated to converge reasonably well to a nearby minimum-energy path, in general crossing one or more saddle points. We use typically 10–20 images, and convergence to a maximum total force per image of 50 meV/Å is reached after 50–100 nudging cycles.

TABLE I. Calculated geometry of the clean and hydrogenated diamond (100)-(2×1) surfaces. The symbol $d_0$ is the equilibrium bulk bond length, $d_{ab}$, etc., are the bond lengths between atoms, labeled according to Fig. 1; $\Delta y_i$ is the lateral displacement along $y=[\bar{1}10]$, $\Delta z_{ij}$ is the interlayer separation, and $\Delta z_i$ the intralayer buckling for monolayer *i*. The length unit is Å.

| | (2×1) | | | (2×1):H | | |
|---|---|---|---|---|---|---|
| | DFTB | LDA [a] | GGA [b] | DFTB | LDA [a] | GGA [b] |
| $d_0$ | 1.544 | 1.529 | 1.548 | | | |
| $d_{Ha}$ | | | | 1.114 | 1.10 | 1.10 |
| $d_{aa}$ | 1.398 | 1.37 | 1.38 | 1.604 | 1.61 | 1.62 |
| $d_{ab}$ | 1.517 | 1.50 | 1.51 | 1.544 | 1.53 | 1.54 |
| $d_{bc}$ | 1.571 | 1.57 | 1.59 | 1.533 | 1.52 | 1.54 |
| $d_{bd}$ | 1.569 | 1.55 | 1.57 | 1.574 | 1.56 | 1.57 |
| $d_{ce}$ | 1.514 | 1.50 | | 1.520 | 1.50 | |
| $d_{df}$ | 1.574 | 1.56 | | 1.565 | 1.55 | |
| $d_{eg}$ | 1.523 | | | 1.527 | | |
| $d_{fg}$ | 1.570 | | | 1.562 | | |
| $d_{gh}$ | 1.542 | | | 1.542 | | |
| $\Delta y_5$ | ±0.05 | | | ±0.03 | | |
| $\Delta y_6$ | ±0.03 | | | ±0.03 | | |
| $\Delta z_{12}$ | 0.704 | 0.67 | | 0.814 | 0.80 | |
| $\Delta z_3$ | 0.249 | 0.26 | | 0.185 | 0.19 | |
| $\Delta z_4$ | 0.145 | 0.16 | | 0.108 | 0.11 | |

[a]Reference 17.
[b]Reference 18.

## III. RESULTS AND DISCUSSION

### A. The clean diamond (100) surface

The clean (100) diamond surface is stabilized by a (2×1) reconstruction characterized by symmetric carbon dimers aligned in chains along a ⟨110⟩ direction. We choose the direction of the principle surface dimer row as [110] and *x* axis, and assign the *z* axis to the surface normal [001].

Table I and Fig. 1 give the geometry for the reference models of the diamond (100)-(2×1) surface, with and without surface hydrogen, as calculated within DFTB,[19] and a comparison with *ab initio* calculations in both the local density approximation[17] (LDA) and the generalized gradient approximation (GGA).[18] The DFTB bulk equilibrium bond

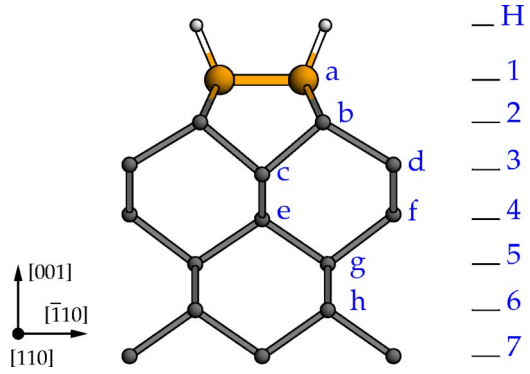


FIG. 1. (Color online) Structure of the diamond (100)-(2×1):H surface. The clean surface is analogous except for the absence of hydrogen. Letters and numbers indicate atoms and monolayers as used in Table I.

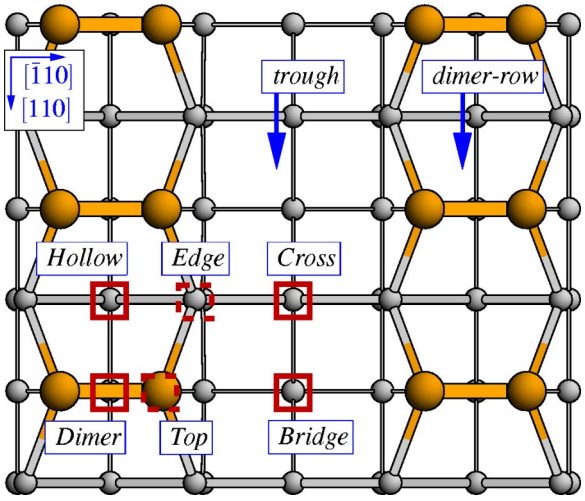


FIG. 2. (Color online) Nomenclature of adsorption sites in the irreducible part of the (100)-(2×1) diamond surface.

length is about 1% larger than the LDA value and essentially matches the more accurate GGA value. The bond lengths of the reconstructed surface follow this pattern. The largest deviations from the GGA results are 0.02 Å for the lengths of the bare surface dimer ($d_{aa}$) and a backbond ($d_{bc}$). This clearly indicates that the SCC-DFTB method reproduces the relaxed geometry extremely well, especially in its most critical features.

The surface energy, defined as energy per surface atom after cleavage, relaxation and reconstruction is 2.29 eV in DFTB, 2.12 eV in LDA,[17] and 1.90 eV in GGA.[18]

### B. Initial $C_2$ deposition

#### *1. Geometry and energetics*

We have systematically investigated a large number of possible configurations for the adsorption of $C_2$ on a clean diamond (100) surface. In the following, we will discuss the geometry and energetics of the most stable isolated adsorbate structures. This is the key to understanding more complex patterns.

To classify the rather large number of ad-dimer configurations we found on this diamond face it is necessary to consider both the adsorption *site* and the ad-dimer *orientation*. Likely adsorption sites are given by the lateral positions of the atoms belonging to the top four monolayers within the (2×1) surface cell. These positions project on the surface an approximately square grid with a lattice constant of half the bulk second-neighbor distance (1.26 Å). Figure 2 identifies six sites within the irreducible part of the surface unit cell using descriptive names, which we adopted following Srivastava and Garrison with a minor variation.[20] We did not find stable positions for $C_2$ at the edge and top sites, which leaves four sites to be discussed further: the dimer (*D*) and hollow (*H*) sites on top of the dimer row, and the bridge (*B*) and cross (*C*) sites along the trough.

Most generally speaking, the ad-dimer orientation will be either in plane or out of plane. We specify in-plane cases as either a parallel (*p*) or orthogonal (*o*) ad-dimer orientation,

TABLE II. Calculated geometry parameters of isolated $C_2$ addimers on the (100)-(2×1) diamond surface (see Fig. 3). Distances given in Å.

| Struct. | Ad-dimer | Ad-dimer surface | Surface [$\bar{1}$10] [a] | Surface [110] [b] | Subsurf. [$\bar{1}$10] |
|---|---|---|---|---|---|
| clean | | | 1.40, 3.64 [c] | 2.52 | 2.34 |
| $D_n$ | 1.29 | 1.50 | 1.55 | | 2.35 |
| $D_p$ | 1.27 | 1.58 | 1.53 | | 2.35 |
| $D_t'$ | 1.30 | 1.90, 1.82, 1.46 [d] | 1.64 | | 2.36 |
| $D_t$ | 1.34 | 1.53, 1.79, 1.39 [d] | 2.12 | | 2.41 |
| $H_p$ | 1.44 | 1.66 | 1.54 | 2.31 | 2.31 |
| $H_o'$ | 1.88 | 1.50 | 1.98 | 2.46 | 2.53 |
| $H_o$ | 1.52 | 1.43 | 2.38 | 2.44 | 2.86 |
| $C_p$ | 1.39 | 1.74 | 1.64, 3.20 [c] | 2.29 | 2.68 [c] |
| $C_o$ | 1.42 | 1.62 | 1.91, 2.69 [c] | 2.40 | 2.58 [c] |
| $B_p$ | 1.23 | 1.50 | 1.63 | | 2.35 |

[a]Dimer direction.
[b]Along dimer row.
[c]Across trough.
[d]Left to right, oriented as in Fig. 3.

referring to the existing surface dimers, while out-of-plane cases give normal (*n*) or tilted (*t*) orientations by referring to the surface plane. By adding the dimer orientation as an index to the site specification we arrive at a nomenclature sufficient for most initial adsorption structures.

Our results for fully optimized geometries of all minimum-energy structures are summarized in Table II and Fig. 3. Further, Table III contains the adsorption energies found in the present work, in comparison with results from previous *ab initio* cluster models on diamond[7] and energies of analogous configurations on the silicon surface.[21]

We identified three groups of configurations for ad-dimers on a clean diamond (100) face after classifying them primarily by their adsorption site. As will be seen, the adsorption energies *do not* reflect the structural ordering.

The first group comprises ad-dimers at the dimer site *D*, each of them is bonded to just one surface dimer. Among the possible ad-dimer orientations we found the normal one (labeled $D_n$) and two tilted orientations ($D_t$, $D_t'$) to be local energy-minima, whereas the parallel orientation ($D_p$) was a saddle point. The structures are depicted in the left row of Fig. 3. We find that $D_t$ has the lowest adsorption energy within this group (−5.43 eV), followed by $D_t'$ and $D_n$ in steps of about 0.3 eV. In contrast, the saddle point configuration $D_p$ is comparatively high, with an energy of 1.2 eV above $D_t$. We found two negative frequency modes, an in-plane rocking mode and a softer twist mode.

The ad-dimer bond lengths in this group are all about 1.3 Å, which is close to the length of a triple bond. These bond lengths, as well as the adatom-to-surface bond lengths agree to within 0.03 Å with those given for similar structures ($D_n$, $D_p$, and $D_t$) in the density functional study by Gruen *et al.*[7] of $C_2$ adsorption on a $C_9H_{12}$ cluster. The DFT and DFTB adsorption energies for the three structures have

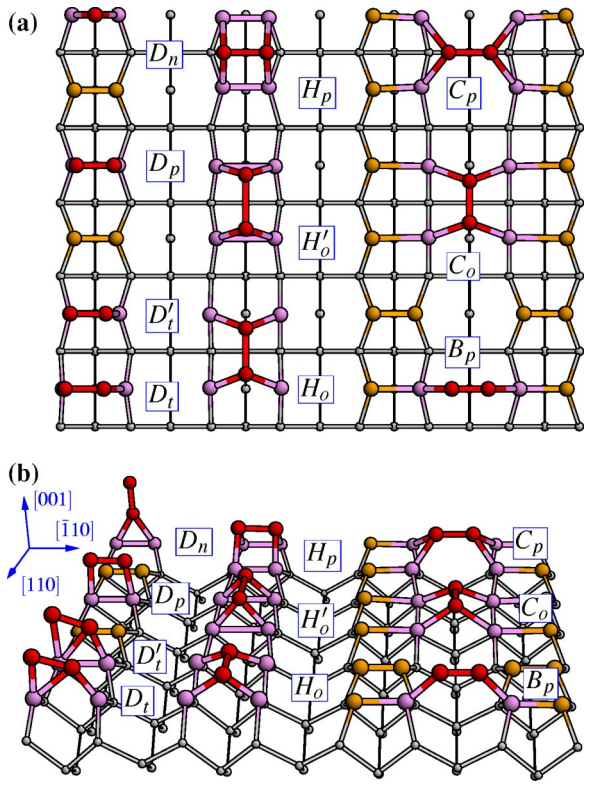


FIG. 3. (Color online) Collage of structures of isolated $C_2$ ad-dimers on the (100)-(2×1) diamond surface. Atoms in the ad-dimer are shown in red (dark). Supplementarily in color online, their first neighbors are shown in magenta. Structures are labeled by adsorption site according to Fig. 2 and the ad-dimer orientation as being parallel (*p*) or orthogonal (*o*) to surface dimers, and normal (*n*) or tilted (*t*) with respect to the surface plane. Bond lengths are given in Table II.

similar trends, but the DFT energies are more negative by 1.0–1.3 eV.

The *D* configurations differ significantly in the length of the surface dimer to which $C_2$ is attached. This surface dimer is only slightly longer than the unperturbed length in the energetically higher structures ($D_n$, $D_p$, and $D'_t$) but it is split to more than 2 Å separation in $D_t$, which makes it the distinguishing feature between the two tilted configurations. Despite the relatively large displacement for the last case, the edge-site atoms on either side of the ad-dimer move away from their undisturbed position by less than 0.1 Å in all cases discussed so far (see the last column in Table II). This finding implies that relatively small finite-cluster models for the adsorption sites consisting just of moveable first neighbor and fixed hydrogen saturated second neighbor carbon atoms (as used for structures 4–6, in Ref. 7) can be expected to give realistic adsorption geometries and energies for such structures. As we will see below, this is not the case in models with ad-dimers bridging two surface dimers, where the edge-site atoms move significantly.

The next group of isolated adsorbate structures are those with the ad-dimer positioned at the hollow site *H* (see Fig. 2), i.e., above a gap along a surface dimer row and bonded to

TABLE III. Energetics of isolated $C_2$ ad-dimers on the (100)-(2×1) diamond surface (see Fig. 3) and comparison with the $Si_2$ ad-dimer on Si. $E_{ads}$ is the energy relative to a separate $C_2$ and a clean surface, and $\Delta E_{ads}$ are energies relative to the minimum of $E_{ads}$. Energies are given in eV.

| | Diamond | | | Silicon | |
|---|---|---|---|---|---|
| Structure | $E_{ads}$ [a] | $E_{ads}$ [b] | $\Delta E_{ads}$ [b] | $\Delta E_{ads}$ [c] | |
| $D_n$ | -6.07 | -4.85 | 2.05 | | |
| $D_p$ | -5.25 | -4.22 | 2.68 | | |
| $D'_t$ | | -5.11 | 1.79 | | |
| $D_t$ | -6.69 | -5.43 | 1.47 | | |
| $H_p$ | | -4.69 | 2.21 | 0.00 | (a) |
| $H'_o$ | | -6.41 | 0.49 | 0.01 | (b) |
| $H_o$ (min.) | | -6.90 | 0.00 | | |
| $C_p$ | | -4.26 | 2.64 | 0.31 | (c) |
| $C_o$ | | -4.65 | 2.24 | 1.11 | (d) |
| $B_p$ | | -6.50 | 0.40 | | |

[a]Reference 7, B3LYP/6-31G* (Table 3).
[b]Present work.
[c]Reference 21, DFT (LDA) plane wave pseudopotential.

two consecutive dimers. There will only be two basic configurations on this site, each with four adatom-to-surface bonds. They are $H_p$ and $H_o$, shown in the middle row of Fig. 3. However, structure $H_o$ appears in two variants with different lengths of the surface dimer. As for $D_t$ discussed above, the lower-energy variant is the one with the surface dimers completely opened. This structure has an adsorption energy of −6.90 eV and is the most stable configuration overall. It represents a continuation of the (100)-(2×1) surface into the next monolayer. This $C_2$ ad-dimer has a bondlength of 1.52 Å and the former surface dimer is opened up to 2.38 Å, which is close to the bulk second-neighbor distance of 2.52 Å. In response, the edge-site atoms below move considerably outwards by 0.26 Å each. Conversely, in the $H'_o$ variant of this structure, a local minimum 0.5 eV higher, the dimer bonds are elongated to just below 2 Å, and the ad-dimer is overstretched to 1.88 Å, while the edge-site atoms move only by 0.10 Å. The bond angles differ greatly between these two structures. In the global minimum structure $H_o$ the angles on the ad-atoms are 112° in the angle facing the former dimer and 109° in the angle facing the dimer gap. While these are nearly tetrahedral, the values for $H'_o$ are 83° and 101°, i.e., far more distorted, which contributes to this structure's higher energy. Implications of the bond length and angle changes for models using small clusters will be discussed in a forthcoming publication.[22]

In the remaining structure of this group, $H_p$, the ad-dimer has a bond length of 1.44 Å and is oriented parallel to the surface dimers, resulting in two roughly square fourfold-rings. The structure is similar to $D_p$. The bond lengths (see Table II) are essentially the same in either case with the exception of the ad-dimer itself, which is 0.2 Å longer. This is easily understood since the ad-atoms in $H_p$ are threefold coordinated, which results in a partial double bond for the ad-dimer as opposed to the (shorter) triple bond seen in $D_p$.

The adsorption energy of $H_p$ is $-4.69$ eV, similar to the structures in the first group. Both the $H_o'$ and $H_o$ structures are much more stable by about 2 eV.

The final group of initial ad-dimer configurations comprises three structures bridging the trough, either at the bridge or the crossover sites. The structures are $B_p$, $C_o$, and $C_p$, and are shown in the rightmost row of Fig. 3.

Among those three, $B_p$ is the most stable, having an adsorption energy of $-6.50$ eV. This is comparable to the value of $-6.90$ eV we found for the global minimum $H_o$, but the bonding structure is completely different. $B_p$ has fewer bonds and introduces a sevenfold ring which is found neither in the bulk lattice nor on the reconstructed surface and thus could constitute a nucleation site.

The other two trough-bridging structures are higher in energy by about 2 eV (see Table III). Their dimer bond lengths are closer to that of a typical double bond, but their backbonds are quite long, especially for $C_p$. In this respect the latter structure is similar to $H_p$. The reason is the proximity of the ad-dimer to their second-neighbor atoms at the edge sites in a strained fourfold ring. The distance mentioned is 2.07 Å for $C_p$ and 2.17 Å for $H_p$; the edge-site atoms have moved vertically inwards by 0.2 Å in either case to accommodate the adsorbate. These geometry effects give rise to a rather high adsorption energy of 2.64 eV. Structure $C_o$ also shows a high energy due to the significant strain of its surface dimers, although the structure is outwardly similar to $H_o$.

#### *2. Bonding*

Two pairs of the configurations described above have only subtle structural differences, namely, $H_o$ compared to $H_o'$ and $D_t$ vs $D_t'$. To understand the reason for the existence of two separate energy minima for these cases we compare their electronic configuration and chemical bonding characteristics on the basis of their Mulliken charges and bond lengths. We find that in the lower-energy structure $H_o$ the ad-dimer is nearly neutral whereas the four base atoms carry a Mulliken charge of about $-0.15\,e$ (i.e., a net negative charge). The situation is reversed for $H_o'$: the ad-atoms have a surplus charge of $-0.24\,e$ each and nearly neutral base atoms. The ad-dimer bond length in $H_o$ indicates a stable single bond, whereas in the local-minimum structure $H_o'$ this bond is more stretched, leading to a dangling bond on each ad-atom. We also observe a rehybridization of edge-site atoms on either side of the ad-dimer for the $H_o$ structure. This type of rebonding does not occur in $H_o'$. The redistribution of charge in the transition between the two structures and accompanying bond changes in the subsurface entail an energy barrier between $H_o$ and $H_o'$ that we determined to be 0.24 eV.

At the dimer site $D$ symmetry breaking lowers the energy of the symmetric configuration $D_p$ by 1.2 eV to the nonsymmetric case $D_t$. The bonding character of the ad-dimer changes from a triple bond to a strained double bond by the formation of a new bond diagonally across the trapezoid formed in the symmetric case.

The structures $D_t'$ and $D_t$ differ only subtly in their electronic configuration. The topmost atoms have charges of $-0.3$ and $-0.4$, respectively. However, in $D_t'$ both atoms of the still intact surface dimer have essentially the same Mulliken charge, whereas in $D_t$ they differ by $0.14\,e$, which is due to the different number of nearest neighbor atoms. Furthermore, the nearly planar threefold coordination for one atom in $D_t$ indicates an $sp^2$ rehybridization.

Structure $B_p$ shows a small bond length of 1.23 Å for the ad-dimer, which clearly indicates a triple bond, and ad-dimer-surface bonds of 1.50 Å length, which equally clearly indicate single bonds. The surface dimers to which it is bonded get slightly stretched to above 1.6 Å. The ad-dimer connects two collinear surface dimers across a trough. This bonding configuration results in a nearly tetrahedral environment for the two adjacent surface atoms and very little stress otherwise. Therefore, this structure is also rather stable.

#### *3. Comparison with silicon*

There is an extensive body of literature discussing the structure and diffusion barriers for silicon dimers on the silicon (100) surface.[21,23–25] It is long known that a simple scaling of low-energy structures from silicon to the shorter diamond bond length does not necessarily yield anything better than a first guess. Silicon relaxes by changes in the bond orientation, whereas carbon relaxes by changes in bonding characteristics. This is reiterated by our present findings. The most stable configurations for the silicon dimers correspond to $H_p$, $H_o'$, $C_p$, and $C_o$, i.e., fully bonded configurations. While we do obtain the analogous global minimum $H_o$ on the diamond surface, this is far from obvious. Table III clearly illustrates the fact that the relevant configurations are much closer in energy on the silicon surface[21] than they are on diamond surfaces.

In particular, the structures $H_p$ and $H_o'$ are essentially isoenergetic on silicon, whereas we found them about 2 eV apart for diamond. One reason is that for silicon these configurations are reconstructed by asymmetric dimer buckling. For $H_p$, this leads to a larger second neighbor distance between the adatoms and edge-site atoms, and in turn to an adsorption energy closer to that of $H_o'$.

Relatively large energy differences of approximately 2 eV between local-minima structures effectively inhibit diffusion on the diamond surface, because as part of a migration from site to site at least one barrier of this height must be overcome. Such events will be rather infrequent at conventional growth temperatures around 500–1000° C. We conclude that ad-dimer diffusion, while a prevalent phenomenon on silicon, is largely absent on diamond.

Another difference between silicon and diamond is that structures with higher bond orders, notably the low-energy structures $H_o$ and $B_p$ do not have stable analogs on the silicon surface, which is ultimately due to the limited ability of silicon to form $\pi$ bonds. Hence, these configurations are unique to carbon.

### C. Barriers

#### *1. Isolated adsorbates*

We have calculated adsorption barriers using the NEB method. For the initial configurations we placed a relaxed

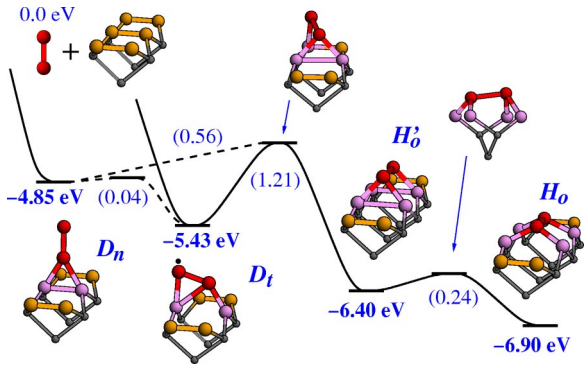


FIG. 4. (Color online) Potential energy surface for $C_2$ adsorption on the clean (100)-(2×1) diamond surface (schematic). Atoms are shown as in Fig. 3. Energies are given in eV; numbers in parentheses are barriers heights.

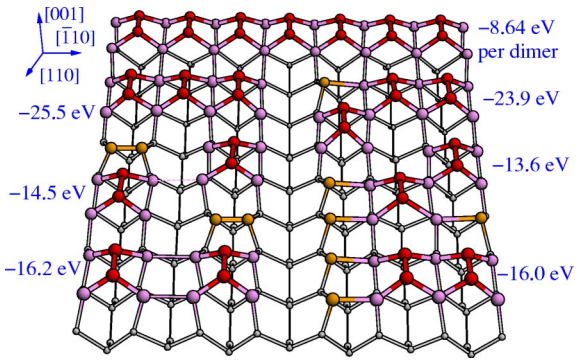


FIG. 5. (Color online) Structure of various $C_2$ ad-dimer clusters on the (100)-(2×1) diamond surface (schematic), illustrating chain growth. Atoms are shown as in Fig. 3. Adsorption energies are given with respect to all $C_2$ in vacuum and a clean surface.

neutral carbon dimer ($C_2$) in a number of orientations well above a relaxed diamond surface at various sites. For the final configurations, we used the structures discussed above. We applied the NEB method to find the closest minimum-energy path between initial and final configurations. This procedure models a dynamic growth process in the limit of a low arrival rate of $C_2$, i.e., each deposition event takes place independently and separate in time. In the following, we discuss the implications for the growth regime.

We actually found no barrier to adsorption for most of the structures identified in the previous section, with the notable exception of the lowest-energy structures $H_o'$ and $H_o$. This is of prime importance to understand the UNCD growth process.

The key results for the adsorption process are summarized in Fig. 4. The following picture emerges: A single $C_2$ dimer arrives at an empty surface dimer site and assumes a normal or tilted orientation, i.e., structures $D_n$ or $D_t$. The normal configuration $D_n$ is unlikely to be present in significant proportion, because asymmetric collision paths which are obviously predominant will lead to $D_t$ directly. Furthermore, there is only a very small barrier of 0.04 eV towards a transformation from $D_n$ to $D_t$. We note that this value is below the accuracy of our method, making this barrier and therefore the stability of structure $D_n$ possibly an artifact.

Both of these $D$ structures are less stable than $H_o'$ and $H_o$. We identified a transition path from $D_t$ to the global minimum configuration $H_o$, which has a relatively high barrier of 1.2 eV. The transition state is characterized by a twist of the ad-dimer towards a neighboring surface dimer, as shown in the center of Fig. 4. After passing the transition state, the local minimum structure $H_o'$ is reached, which then converts to $H_o$ with a relatively low barrier of 0.24 eV.

The adsorption to the second low-energy structure $B_p$ proceeds without barrier. The remaining structures considered all have a formation energy at least 2 eV higher and will not be discussed further.

In summary, the most populated configurations for isolated ad-dimers on the diamond (100) face will be the tilted dimer-bridge ($D_t$), the parallel trough bridge ($B_p$), and the orthogonal dimer bridge ($H_o$). Only the first two are reached without barrier and are topologically imperfect and may therefore constitute re-nucleation sites. This has important implications for the kinetics of growth, which will be addressed in detail in a separate publication.[26]

### *2. Joined adsorbates*

We now consider the case when ad-dimers are not isolated on the surface, but occupy neighboring sites. Given the variety of the single-dimer structures discussed so far and the well-known variability of carbon in general a complete analysis would far exceed the scope of this study. We can only illustrate a few examples which we believe are typical and provide sufficient grounds for drawing conclusions.

First, Fig. 5 represents the ideal case of coadsorption of dimers into neighboring $H_o$ and $C_o$ sites, leading to chain growth by advancing $S_B$-type[27] step edges, i.e., single layer steps parallel to the dimer bond in the adsorbate layer. Step advancement proceeds in two key processes. The first is adsorption into a trough site $C_o$ next to an on-top dimer $H_o$. This proceeds *without* a barrier, resulting in the structure shown at the bottom right of Fig. 5. The surface dimers adjacent to the filled trough become elongated to 1.8 Å and the outer atoms are slightly charged, making this hollow site reactive. As a result, a subsequent dimer adsorption into this site, which completes the $S_B$ step advancement, has a very low barrier of 0.1 eV. Chain growth is therefore possible. Nonetheless, positional disorder can arise when dimers adsorb at the step edge or on a neighboring dimer row site out of registry for the new (2×1) monolayer. This disorder may well persist until coverage is complete. The formation energy for a single line defect on the surface due to a lateral stacking fault is $\approx$0.3 eV per dimer.

The chain growth model requires a seed in the ideal bonding configuration. However, since we found that the prevalent configurations for isolated dimers are *not* the ideal ones, we need to consider the implications for higher surface coverage. We selected the lowest-energy configurations that are reached without a barrier, and calculated structures arising from their pairing, i.e. $D_t+B_p$, $D_t+D_t$, and $B_p+B_p$.

For the mixed case, we found that the barrier for transition from $D_t$ to the growth position $H_o$ is lowered from 1.2

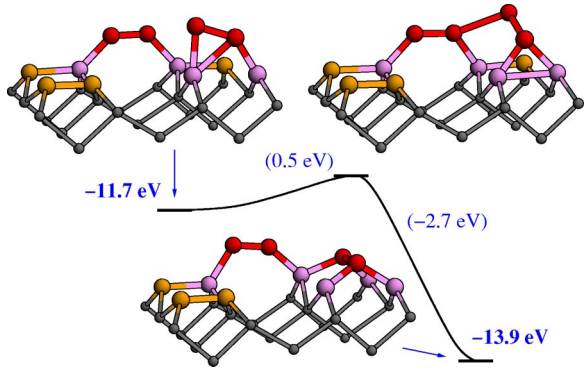


FIG. 6. (Color online) Transition path for $D_t \rightarrow H_o$ with a neighboring $B_p$ structure. The barrier is lower than for an isolated $D_t$ structure (see Fig. 4). Atoms are shown as in Fig. 3.

eV (Fig. 4) to 0.5 eV in the presence of a trough-bridging dimer ($B_p$) due to the formation of an intermediate bond, as shown in Fig. 6. For the related situation, with the $D_t$ dimer tilted in the opposite orientation than shown in the figure, the barrier is 0.8 eV.

The insertion of the next ad-dimer on the other side of the trough into an $H_o$ configuration proceeds largely through the same mechanism as the first one. However, we found that in the process, the structure $B_p$, being the second dominant isolated dimer structure, now sandwiched between two $H_o$ dimers, becomes unstable. Under these circumstances, the trough narrows due to the breaking of the original surface dimers, and the ad-dimer across the trough assumes a surface-normal orientation, shown in Fig. 7 (top left). This upright configuration, labeled $B_n$, easily converts into the ideal trough-filling position $C_o$ with a barrier of 0.6 eV. Therefore, structure $B_p$ can ultimately lead to growth and does not necessarily constitute a nucleation site.

The reaction pathway in Fig. 7 also represents the case of an extended dimer row with a single-dimer gap, as would be found on a nearly complete surface. The geometries and especially the reaction barrier are essentially the same as for three ad-dimers, i.e., the case illustrated in Fig. 7. This has

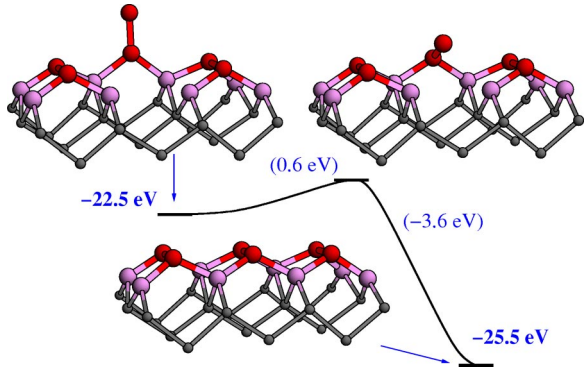


FIG. 7. (Color online) Transition path $B_n \rightarrow C_o$, completing chain growth by filling a trough site. The initial structure is reached without barrier by either an adsorption of a dimer in a bridge site or a conversion from $B_p$ following the adsorption of nearby $H_o$ structures, similar to Fig. 6. Energies are adsorption energies for three $C_2$'s relative to a clean surface.

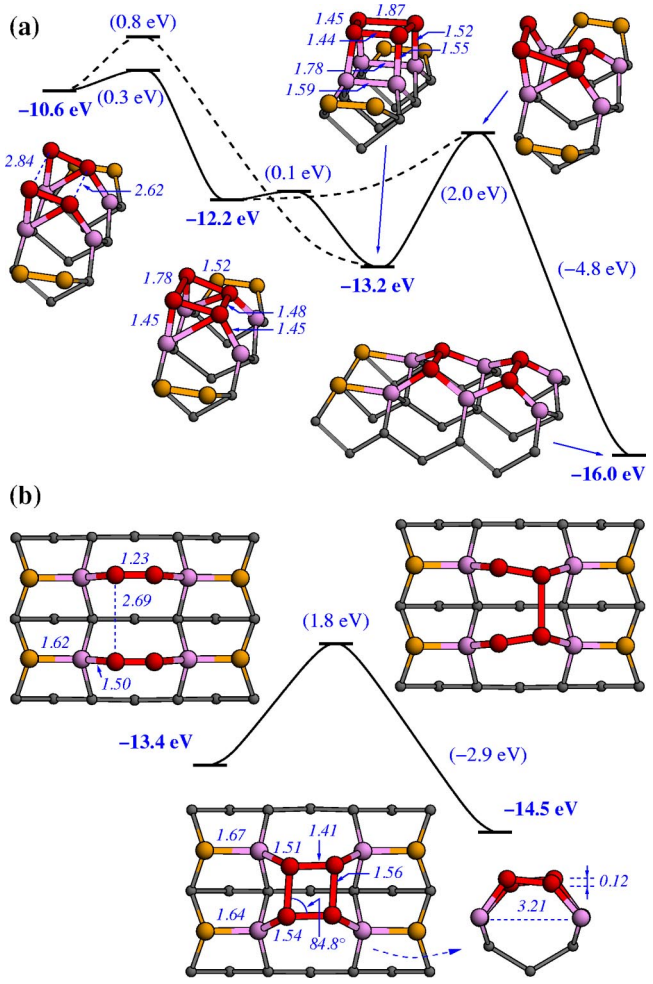


FIG. 8. (Color online) Structures resulting from an agglomeration of (a) two $D_t$ and (b) two $B_p$ configurations (see text). Energies are adsorption energies for two $C_2$'s relative to a clean surface. Numbers in parentheses are barriers heights. Bond lengths are given in Å.

the consequence that the reverse reaction, leading to a breakup of an extended surface, has a barrier of well over 3 eV. Therefore, the reverse reaction, which would introduce a surface defect, is extremely rare under common growth conditions, and hence the surface is stable.

The pathways for an agglomeration of two tilted ad-dimers, i.e., the case $D_t + D_t$, are more complicated and are shown in Fig. 8(a). Two initially separate adsorbates can form a rather stable $C_4$ agglomerate on the surface after overcoming relatively small barriers of 0.3 and 0.1 eV. The agglomerate can be described as two fused $D_p$ adsorbates with unequal bond lengths. Details on the geometry of this structure are included in Fig. 8. Most importantly, the barrier leading away from this structure towards a topologically perfect $C_oH_o$ arrangement, is 2.0 eV, which is rather high. Therefore, the agglomerate is likely a renucleation site.

A similar $C_4$ aggregate is formed from the combination of two trough-bridging dimers $B_p + B_p$, which is the last of the simple cases we will discuss here. The structure is shown in Fig. 8(b). In contrast to the previous case, however, this aggregate has a much higher formation barrier. For two $B_p$

placed in adjacent sites, the close proximity of $\pi$ bonds between the dimer atoms gives rise to a slight repulsion until the dimers reach an equilibrium distance of 2.7 Å in the initial structure. The bulging in the initial structure also occurs in the case of $D_t+D_t$ above, but given the asymmetric charge distribution and additional neighbor atoms the $\pi$ bonding is weaker and hence the barrier is much lower for that case. For the present case, the $\pi$-$\pi$ interaction is stronger and gives rise to a high barrier of 1.8 eV towards fusing the $B_p$ dimers. As a result, $B_p$ dimers are unlikely to merge, but instead will go one by one through the path shown in Fig. 7. Therefore, the trough-bridging configuration $B_p$, although initially a non-growth orientation, most likely ultimately leads to growth.

### D. Implications for growth

In the previous section, we found that adsorption channels on the hydrogen-free diamond (100) surface which lead to growth positions face relatively large barriers of $>1$ eV for isolated adsorbates, and a somewhat lower barrier of 0.5 $-0.8$ eV towards growth for combined adsorbates involving trough-bridging configurations. Conversely, neighboring adsorbates on a dimer row form defect agglomerates through low barriers. The agglomerates in turn have high barriers of $\approx 2$ eV towards conversion into growth positions and therefore constitute renucleation sites.

The findings discussed here confirm and extend those discussed before for the case of isolated dimers.[7] For the present work we have studied more configurations, in particular paired structures, and can clearly show that both renucleation and growth occurs on the (100) diamond face.

This is in stark contrast to the situation on the (110) face.[12] There, essentially only one adsorption channel existed for $C_2$, and this channel led directly to growth in a lattice site orientation. While this does of course not rule out renucleation on the (110) surface, it is noteworthy that most subsequent adsorption events we found did lead to growth.

So far, we have not studied the (111) face in this context. Experimentally, this face is found to dehydrogenate at temperatures above 1050–1150 K, (Ref. 28) and to transform into the (111)-(2×1) Pandey-chain reconstruction.[29] It is interesting to note that the reconstruction is similar in geometry to the unreconstructed but stable (110)-(1×1) face. For both faces, polyethylenelike zigzag chains are characteristic, separated by troughs of the same zigzag chain type. Therefore, one would expect related adsorption mechanisms on both faces. There are, however, two key differences which complicate the situation: (a) the trough for the Pandey chain reconstruction is wider (3.7 Å vs 2.9 Å) and more shallow than for the (110) face, and (b) the backbond configuration on the (110) face is bulklike, i.e., shows sixfold rings, whereas on the Pandey chain the backbonds involve fivefold and sevenfold rings instead. This means that for bulk growth on this surface, bond switching must take place. Thermally induced dereconstruction has been observed at temperatures around 1100–1275 K, see Refs. 28,30, which is only about 100–200 K above the growth temperature. Furthermore, point (a) makes the surface more susceptible to graphitization. A recent *ab initio* study has addressed some of these points.[31] The authors suggest a growth path for Pandey chains starting with an the unreconstructed surface and leading to a graphite adlayer. Given the temperature-induced changes in bonding, however, questions remain to be answered for the (111) surface to fully understand the $C_2$ growth mechanism on all diamond faces.

The present results complement our previous work on the (110) face.[12] Our findings would seem to confirm observations that, as in the methyl-based growth, the (110) face is the fastest growing one in the $C_2$ regime as well, while (100) faces are slow growing, constitute sites for renucleation, and lead to 100-like grain boundaries. However, the results suggest that reactions leading to both growth and renucleation are possible, which helps to understand observed small grain sizes in UNCD. To complete the picture, a careful evaluation of the influence of experimental conditions is also necessary. In particular, surface hydrogen may play a significant role.

## IV. SUMMARY AND CONCLUSIONS

We have simulated diamond growth steps by studying isolated and agglomerated $C_2$ molecules adsorbed on a reconstructed nonhydrogenated diamond (100)-(2×1) surface. Our results are as follows.

(1) The most stable configuration (labeled $H_o$) is a bridge between two adjacent surface dimers along a dimer row. The surface dimers themselves are opened. The configuration has an adsorption energy of $-6.9$ eV and a barrier of 1.2 eV must be overcome to reach it on a clean surface.

(2) There are many other configurations with adsorption energies differing by up to 2.7 eV. We found a number of adsorption structures, revealing a complex energy landscape and consequently many adsorption channels. By comparison, analogous structures for silicon are closer in energy and less varied because Si lacks $\pi$ bonding.

(3) Also in contrast to silicon, which has diffusion barriers for dimers on the surface of the order of 1 eV, the barriers on the (100) diamond surface are much higher, about 2–3 eV, effectively precluding diffusion on the surface at experimental growth temperatures. This is a direct consequence of larger energy differences between various adsorption structures for $C_2$ on diamond. These results once again illustrate that surface properties cannot simply be scaled from silicon to diamond, even though they share the same crystal structure.

(4) Multiple $C_2$ species result in various agglomerate structures, giving rise to complex adsorption patterns. In particular, both growth *and* nucleation are possible.

## ACKNOWLEDGMENTS

We thank P. Maragakis, Harvard University, for contributions in interfacing DFTB with the NEB method. This work is supported by the U.S. Department of Energy, BES-Materials Sciences, under Contract No. W-31-109-ENG-38.

*Electronic address: email sternberg@anl.gov

[1] S. J. Harris and D. G. Goodwin, J. Phys. Chem. **97**, 23 (1993).
[2] M. P. D'Evelyn, in *Handbook of Industrial Diamonds and Diamond Films*, edited by M. A. Prelas, G. Popovici, and L. K. Bigelow (Marcel Dekker, New York, 1997), Chap. 4, pp. 89–146.
[3] R. C. Brown, C. J. Cramer, and J. T. Roberts, J. Phys. Chem. B **101**, 9574 (1997).
[4] H. Tamura, H. Zhou, Y. Hirano, S. Takami, M. Kubo, R. V. Belosludov, A. Miyamoto, A. Imamura, M. N. Gamo, and T. Ando, Phys. Rev. B **62**, 16 995 (2000).
[5] D. M. Gruen, Annu. Rev. Mater. Sci. **29**, 211 (1999).
[6] D. M. Gruen, S. Liu, A. R. Krauss, J. Luo, and X. Pan, Appl. Phys. Lett. **64**, 1502 (1994).
[7] D. M. Gruen, P. C. Redfern, D. A. Horner, P. Zapol, and L. A. Curtiss, J. Phys. Chem. B **103**, 5459 (1999).
[8] P. Keblinski, D. Wolf, F. Cleri, S. R. Phillpot, and H. Gleiter, MRS Bull. **23**, 36 (1998).
[9] P. Zapol, M. Sternberg, L. A. Curtiss, Th. Frauenheim, and D. M. Gruen, Phys. Rev. B **65**, 045403 (2002).
[10] D. A. Horner, L. A. Curtiss, and D. M. Gruen, Chem. Phys. Lett. **233**, 243 (1995).
[11] P. C. Redfern, D. A. Horner, L. A. Curtiss, and D. M. Gruen, J. Phys. Chem. **100**, 11654 (1996).
[12] M. Sternberg, M. Kaukonen, R. M. Nieminen, and Th. Frauenheim, Phys. Rev. B **63**, 165414 (2001).
[13] D. Porezag, Th. Frauenheim, Th. Köhler, G. Seifert, and R. Kaschner, Phys. Rev. B **51**, 12 947 (1995).
[14] Th. Frauenheim, G. Seifert, M. Elstner, Z. Hajnal, G. Jungnickel, D. Porezag, S. Suhai, and R. Scholz, Phys. Status Solidi B **217**, 41 (2000).
[15] G. Mills and H. Jónsson, Phys. Rev. Lett. **72**, 1124 (1994).
[16] H. Jónsson, G. Mills, and K. W. Jacobsen, in *Classical and Quantum Dynamics in Condensed Phase Simulations*, edited by B. J. Berne, G. Ciccotti, and D. F. Coker (World Scientific, Singapore, 1998), pp. 385–404.
[17] J. Furthmüller, J. Hafner, and G. Kresse, Phys. Rev. B **53**, 7334 (1996).
[18] J. A. Steckel, G. Kresse, and J. Hafner, Phys. Rev. B **66**, 155406 (2002).
[19] M. Sternberg, Ph.D. thesis, Fachbereich Physik, Universität Paderborn, Germany (2001).
[20] D. Srivastava and B. J. Garrison, Phys. Rev. B **95**, 6885 (1991).
[21] G. Brocks and P. J. Kelly, Phys. Rev. Lett. **76**, 2362 (1996).
[22] M. Sternberg, P. Zapol, and L. A. Curtiss (unpublished).
[23] T. Yamasaki, T. Uda, and K. Terakura, Phys. Rev. Lett. **76**, 2949 (1996).
[24] G.-D. Lee, C. Z. Wang, Z. Y. Lu, and K. M. Ho, Phys. Rev. Lett. **81**, 5872 (1998).
[25] C.-C. Fu, M. Weissmann, and A. Saul, Surf. Sci. **481**, 97 (2001).
[26] P. Zapol and M. Sternberg (unpublished).
[27] D. J. Chadi, Phys. Rev. Lett. **59**, 1691 (1987).
[28] H.-G. Busmann and I. V. Hertel, Carbon **36**, 391 (1998).
[29] K. C. Pandey, Phys. Rev. Lett. **47**, 1913 (1981).
[30] P. G. Lurie and J. M. Wilson, Surf. Sci. **65**, 453 (1977).
[31] S. W. Yang, X. Xie, P. Wu, and K. P. Loh, J. Phys. Chem. B **107**, 985 (2003).